JCTC Journal of Chemical Theory and Computation

ARTICLE

pubs.acs.org/JCTC

Self-Consistent-Charge Density-Functional Tight-Binding Parameters for Cd−X (X = S, Se, Te) Compounds and Their Interaction with H, O, C, and N

Sunandan Sarkar,[†] Sougata Pal,[†,‡] Pranab Sarkar,[*,†] A. L. Rosa,[§] and Th. Frauenheim[§]

[†]Department of Chemistry, Visva-Bharati University, Santiniketan- 731235, India

[‡]Institute of Theoretical Physics and Astrophysics, University of Kiel, D-24098, Kiel, Germany

[§]BCCMS, University of Bremen, Am Fallturm 1, 28359, Bremen, Germany

ABSTRACT: Parameters for CdX, SeX, and TeX (X = H, C, N, O, S, Se, Te, and Cd) have been generated within the self-consistent-charge density-functional tight-binding (SCC-DFTB) framework. The approach has been tested against ab initio density-functional theory calculations for the relevant bulk phases, surfaces, nanowires, and small molecular systems. The SCC-DFTB approach reproduces structural, electronic, and energetic properties very well, demonstrating that the developed parameters are fully transferable among different chemical environments.

1. INTRODUCTION

During the past couple of decades, nanostructured materials have been a very exciting field of research.[1−5] The impact of this research on both fundamental science and potential applications has been tremendous and is still rapidly growing. The interest in this particular class of materials stems from the fact that their properties can be tuned by varying either their size or shape. The emphasis has been mainly on II−VI and III−V semiconductors, which show strong confinement effects. II−VI semiconductors are particularly interesting and have been the focus of many experimental[6−23] and theoretical studies[24−47] in the recent past. The strong size- and shape-dependent optical properties of these materials have led to their use in optoelectronic devices[8,11−18,18−20] and as biological tags.[9,21−23] CdS is one of the direct wide-gap semiconductor with good stability and high luminescence properties. Because of its high photosensitivity and attractive applications in photoconducting cells, CdS nanoparticles have been studied as model photoconductors. CdS nanostructures such as nanowires, nanorods, and nanodots have been grown experimentally, and they have been applied in photovoltaic cells, photonic switches, and optoelectronic devices.[6,7] Recently, CdS nanostructures have also been used in biolabeling, imaging, drug delivery, and other biotechnological areas.[8−10] CdSe is one of the most extensively studied quantum nanostructured materials due to its strong size-tunable properties. Hence, it is a good candidate for optic-related applications, including solar cells and photoelectrochemical (PEC) cells.[11−18] CdTe has proven to provide good optical performance across a wide range of temperatures and has provided adequate mechanical robustness to be used as substrate materials. Self-assembled CdTe nanodots have high efficiency in terms of photoluminescence and hence are appropriate candidates for the purpose of making LEDs.[20] Very recently, semiconductor quantum dots of CdSe and CdTe with their tunable band edges offer new opportunities for harvesting light energy in the visible region of the solar spectrum.[48−50] The use of CdSe and CdTe quantum dots facilitates charge separation and the generation of photo currents under visible light irradiation. A further area of concentration focuses on shape-controlled II−VI nanomaterials with recently reported structures comprising nanowires, nanocables, nanoribbons, and nanorods.[51−54] There are relatively few reports involving the preparation of ternary II−II′−VI nanomaterials.[55−60] In these alloyed compounds, manipulation of the band gap energy can be achieved by changing both particle size and composition (i.e., the ratio of M to M′). Recently, this has been demonstrated with the synthesis of a series of highly luminescent $Zn_xCd_{1-x}Se$ nanocrystals whose emission energy can be tuned across the visible spectrum by increasing the Zn/Cd ratio.[61] Thus, the development of new approaches to access ternary nanoparticles is an attractive pursuit. So exploration of size-, composition-, and shape-tunable electronic structures of this class of materials is still an active field of research from both experimental and theoretical points of view.

Due to the interest in the variation of the electronic properties as a function of the system size and shape, there have been a number of theoretical studies devoted to the properties of various kinds of cadmium chalcogenide nanostructures. Obviously, the highest accuracy is achieved by the *first-principle* methods, but because of their high computational demands, they become prohibitive to simulating a large number of atoms. In addition to numerous traditional quantum mechanical methods, self-consistent-charge density-functional tight-binding (SCC-DFTB) schemes have also been very successful[62−66] in treating large systems. In many cases, the results of these two-center-oriented schemes deviate only slightly from those of more sophisticated methods. Therefore, the SCC-DFTB method has been applied to simulate a large number of atoms quantum mechanically in the fields of nanotechnology and solid state physics. Very recently, Bhattacharya et al. developed TB parameters for CdS and ZnS by fitting the TB band structure to the full potential linear augmented plane wave (FP-LAPW) band

Received: April 16, 2011
Published: June 16, 2011

structure.[67] In this work, we report the development of SCC-DFTB parameters for various cadmium chalcogenides [CdX, X = S, Se, and Te] and their interactions with C, O, N, and H. Our parameters have been validated against density-functional theoretical (DFT) calculations for bulk, surfaces, nanowires, and small molecules. We also compare the SCC-DFTB results with the available experimental results. We show that our parameters are able to reproduce atomic geometries, binding energies, and energy dispersion quite well in comparison with first-principle calculations, demonstrating good transferability among different chemical environments.

2. COMPUTATIONAL METHODOLOGY

2.1. SCC-DFTB Approach. The self-consistent charge density-functional method used in this work has been described in detail elsewhere.[62−66] Therefore, we just give a brief overview of the method. In SCC-DFTB method, the total energy can be expressed as a second order expansion of the DFT Kohn−Sham[68,69] total energy with respect to charge density fluctuations.

$$E_{\mathrm{tot}}^{\mathrm{DFTB}} = \sum_{i}^{\mathrm{occ}} n_i \langle \Psi_i | \hat{H}_0 | \Psi_i \rangle + \frac{1}{2} \sum_{\alpha\beta}^{N} \gamma_{\alpha\beta} \Delta q_\alpha \Delta q_\beta + E_{\mathrm{rep}}$$

$$= E_0[n_0] + E_2[n_0, \delta n] + E_{\mathrm{rep}} \quad (1)$$

The first term of eq 1 is the sum over the occupied eigenstates Ψ_i of the effective Kohn−Sham Hamiltonian $\hat{H}_0$, derived under the approximation that the initial electronic density of the many-atom system can be represented as a superposition of corresponding neutral atomic charge densities (n_0). This Hamiltonian is also subjected to the frozen-core approximation, i.e., only the valence electrons are treated explicitly whereas the inner electrons are represented by an effective (pseudo) potential. The second term, E_2, corresponds to the second-order expansion of the exchange-correlation functional with respect to charge density fluctuations δn (the first-order terms in this expansion vanish for any arbitrary n_0), approximated as atomic point like charges (Δq) together with an analytical interpolating function $\gamma_{\alpha\beta}$. This term is important for our cadmium chalcogenide systems, as there are electronegativity differences between the cadmium and chalcogenides. Finally, the third term, E_{rep}, accounts for the "double-counting" terms and the ion−ion core interaction in a set of distance-dependent pairwise repulsive potentials, modeled as the difference between the SCC-DFTB electronic energy ($E_{\mathrm{Elec}}^{\mathrm{DFTB}} = E_0 + E_2$) and the total DFT energy for some reasonably chosen reference system.

The wave functions (Ψ_i) are expanded as a linear combination of atomic orbitals:

$$\Psi_i = \sum_n c_n \phi_n \quad (2)$$

The Kohn−Sham atomic orbitals ϕ_n, in eq 2 are constructed as a linear combination of Slater-type orbitals, obtained by solving the following Kohn−Sham equation for the spin-unpolarized free atom self-consistently:

$$\left[\hat{T} + v_0 + \left(\frac{r}{r_0} \right)^2 \right] \phi_n(r) = \varepsilon_n \phi_n(r) \quad (3)$$

The modified Hamiltonian in eq 3 consists of a kinetic energy operator $\hat{T}$, the potential energy for the neutral atom v_0, and an additional harmonic potential $(r/r_0)^2$ used to enforce the localization of the atomic orbitals and to improve the quality of the energy band structures. Having defined the atomic orbitals (ϕ) and an initial set of expansion coefficients (c_n), we estimated the atomic charge fluctuations (Δq) via Mulliken population analysis, and the DFTB total energy problem is solved self-consistently by using the following secular equation:

$$\sum_i c_{in}(H_{nm} - \varepsilon_i S_{nm}) = 0 \quad \forall \quad n, i \quad (4)$$

with

$$H_{nm} = H_{nm}^0 + \frac{1}{2} S_{nm} \sum_{\eta}^{N} (\gamma_{\alpha\eta} + \gamma_{\beta\eta}) \Delta q_\eta$$

$$H_{nm}^0 = \langle \phi_n | \hat{H} | \phi_m \rangle \quad \forall \quad n \in \alpha, m \in \beta$$

$$S_{nm} = \langle \phi_n | \phi_m \rangle$$

In eq 4, the diagonal zero-order matrix elements H_{nm}^0 are taken as the eigenvalues obtained from the free atom calculations, while the distance-dependent nondiagonal elements H_{nm}^0 and S_{nm} are calculated within the two-center approximation. These values are tabulated over a large number of interatomic distances that allows one to obtain interpolated values at any distance and thus avoids integral evaluations during DFTB calculations leading to a computational efficiency comparable to those of traditional semiempirical methods while retaining the accuracy. The charge transfer among different atoms takes into account their respective chemical hardness (Hubbard parameters), calculated as the first derivative of the total atomic energy with respect to the electronic occupation around the neutral-atom electronic density.

The necessary parameters to represent a system within the DFTB method include the Hamiltonian and overlap matrix elements (H_{nm}^0 and S_{nm}), Hubbard parameters for every chemical element, and the repulsive pairwise potentials for all interacting neighbors. The successful SCC-DFTB parametrization implies that the main energetic and structural properties are well reproduced with respect to either DFT or the experiment. This can be achieved by adjusting the wave function and density confinement radii for a given element as well as by accurate construction of repulsion profiles. The required properties of any atom in the SCC-DFTB framework include the LCAO basis functions χ_μ, the reference input density (n_0), the wave function confinement radius (r_0), and the chemical hardness parameters, U_A. The LCAO basis functions χ_μ are obtained from atomic Kohn−Sham calculations with the PBE exchange-correlation functional, which was derived by Perdew, Burke, and Ernzerhof, in the presence of the harmonic potential, $(r/r_0)^2$.[70] It forces the wave functions to avoid areas far away from the nucleus, thus resulting in an electron density that is compressed in comparison to the free atom. The good choice for r_0 values is $r_0 \approx 2r_{\mathrm{cov}}$, where r_{cov} is the covalent radius of the element. The r_0 values are chosen to be 3.0, 2.8, and 2.8 bohr corresponding to s, p, and d functions of cadmium. For selenium, r_0 values are 3.4, 5.3, and 5.4 bohr corresponding to s, p, and d functions, and the r_0 values of tellurium are 3.0, 6.8, and 6.4 bohr corresponding to s, p, and d functions. Another atomic property, the reference input density (n_0), is chosen to be 8.2, 10.0, and 11.0 bohr for the corresponding elements Cd, Se, and Te. These parameters have been selected out of a large number of trials and ensure that SCC-DFTB reproduces accurate DFT electronic band structures for solid-state elements to the highest possible degree. In the case of

Table 1. Parametrization Details of the Pairwise Repulsive Potentials for Cd−X, Se−X, and Te−X Interactions (X = H, C, N, O, S, Se, Te, and Cd)

	reference	repulsive	bond distance (Å)	
interaction	system	cutoff (Å)	SCC-DFTB	PP-PBE
Cd−H	CdH_2	1.90	1.76	1.76
Cd−C	CdC	2.38	2.16	2.19
Cd−N	CdN	2.38	2.22	2.39
Cd−O	CdO	2.12	1.89	1.94
Cd−S	zb-CdS	2.80	2.56	2.60
Cd−Se	zb-CdSe	2.96	2.61	2.71
Cd−Te	zb-CdTe	3.17	2.80	2.89
Cd−Cd	fcc-Cd	4.17	3.25	3.21
Se−H	SeH	1.59	1.51	1.51
Se−C	SeC	2.12	1.71	1.71
Se−N	SeN	2.12	1.71	1.70
Se−O	SeO	3.02	1.72	1.71
Se−S	SeS	2.86	2.05	2.10
Se−Se	Se_2	3.23	2.34	2.53
Te−H	TeH	1.80	1.70	1.72
Te−C	TeC	2.65	1.94	1.95
Te−N	TeN	2.59	1.93	1.95
Te−O	TeO	3.00	1.95	1.94
Te−S	TeS	3.00	2.33	2.32
Te−Se	TeSe	3.17	2.50	2.49
Te−Te	Te_2	3.81	3.02	3.10

other elements (H, C, N, O, S), we have employed the same initial atomic parameters as have been reported earlier.[63]

Repulsion profiles for Cd−X (X = H, C, N, O, S, Se, Te, and Cd), Se−X (X = H, C, N, O, S, Se), and Te−X (X = H, C, N, O, S, Se, and Te) pairs at a series of interatomic distances (R) were generated by fitting them with cubic splines of the difference of DFT total energy and the electronic DFTB energy against distance in a simple reference system. Repulsion profiles for different pairs are characterized by different cutoff values, indicating the distance at which the repulsion energy approaches zero. The brief overview of parametrization details used for the generation of Cd−X, Se−X, and Te−X repulsion profiles are summarized in Table 1.

The SCC-DFTB calculations were carried out with the DFTB + code.[66] The bulk properties of rock-salt CdO and zinc-blende (zb) CdX (X = S, Se, and Te) are calculated using the periodic boundary condition (PBC) and used an 8 × 8 × 8 Monkhorst−Pack (MP)[71] grid for k-point sampling. For hcp-Cd and wurtzite (wz) CdX (X = S, Se, and Te), we used an 8 × 8 × 4 MP grid for k-point sampling. We used 5 × 5 × 5 MP grids for k-point sampling to study trigonal bulk Se and Te.

2.2. Benchmark DFT Calculations. As a reference for the performance of the SCC-DFTB methods, we use the GGA-PBE functional, as implemented in SIESTA package[72] using a double-ζ plus polarization function (DZP) basis set for the Cd atom; a double-ζ function (DZ) basis set for H, C, N, O, S, Se, and Te atoms; and norm-conservative Troullier−Martins pseudopotentials (PP)[73] for representing the valence and inner electrons, and also a B3LYP functional[74,75] with an SBK basis set for Cd, Se, and Te and 6-31G(d,p) for H, C, N, O, and S, as implemented in the Gaussian 03 package.[76] In the case of bulk systems like face-centered (fcc), hexagonal close packing (hcp), trigonal, rock-salt, zinc-blende (zb), and wurtzite (wz), PP-PBE calculations were performed with periodic boundary conditions (PBC). For the fcc-Cd, rock-salt CdO, and zb-CdX (X = S, Se, and Te) solid-state reference systems, the k-points were sampled with an 8 × 8 × 8 grid. For hcp-Cd and wz-CdX (X = S, Se, and Te), the k-points were sampled with an 8 × 8 × 4 grid and, for trigonal Se and Te, a 5 × 5 × 5 Monkhorst-Pack (MP)[71] grid and using the 225 Ry Mesh cutoff. For the calculation of $(10\bar{1}0)$ and $(11\bar{2}0)$ surfaces, the k-points were sampled with 6 × 1 × 4 and 1 × 4 × 4 MP grids, respectively, with a 225 Ry Mesh cutoff. The $(10\bar{1}0)$ and $(11\bar{2}0)$ faceted nanowires were calculated using a 1 × 1 × 4 MP grid for k-point sampling. For molecular reference systems, the calculations were performed by employing large supercells, including a 15 Å vacuum region in all directions to isolate the molecules from their periodic replicas.

Table 2. Structural and Energetic Properties of Bulk Phases of Cd, Se, and Te Calculated Using SCC-DFTB and PP-PBE (Experimental Values Are Also Given)

	c (Å)	a (Å)	c/a	B (Gpa)	E_c (eV/atom)	E_g (eV)
hcp Cd						
SCC-DFTB	5.58	2.96	1.88	76.40	1.41	
PP-PBE	5.72	3.08	1.86	42.93	1.24	
exptl[a]	5.62	2.98	1.89	46.70	1.16	
trigonal Se						
SCC-DFTB	5.18	4.39	1.18	49.15	2.63	1.49
PP-PBE	5.18	4.54	1.14	39.48	2.26	0.84
exptl[b]	4.96	4.37	1.14	14.90	2.25	1.98
trigonal Te						
SCC-DFTB	6.26	4.85	1.29	50.95	2.21	0.68
PP-PBE	6.05	4.55	1.33	28.33	2.19	0.19
exptl[c]	5.93	4.45	1.33	23.00	2.19	0.33

[a] Refs 77−79. [b] Refs 79 and 80. [c] Refs 81 and 82.

3. RESULTS AND DISCUSSION

3.1. Bulk hcp-Cd and Trigonal Se and Te. We have determined the lattice parameters and elastic properties of bulk hcp-Cd and bulk trigonal selenium and tellurium by calculating energy-volume profiles in a ±15% range around the experimental equilibrium volumes and fitting the results to the Murnaghan equation of state. Like other studies we have not fixed the value of the c/a ratio; rather we have also optimized it. In our calculation, the internal parameter u (in Å) for selenium and tellurium was taken as 0.2285 and 0.2640, respectively. The equilibrium lattice parameters and energetic properties of the cadmium hcp bulk phase and trigonal phases of selenium and tellurium obtained using SCC-DFTB and PP-PBE together with experimental values are shown in Table 2. As is evident from Table 2, the DFTB parameters except the bulk modulus for all considered bulk systems are in fairly good agreement with the PP-PBE and experimental results.[77−82] As expected, the values of cohesive energies are little higher than the corresponding DFT and experimental results because the DFTB calculation overestimates this property. The large error in bulk modulus is because of the fact that we have used strong wave function compression for these elements, which lowers their electronic energy wells.

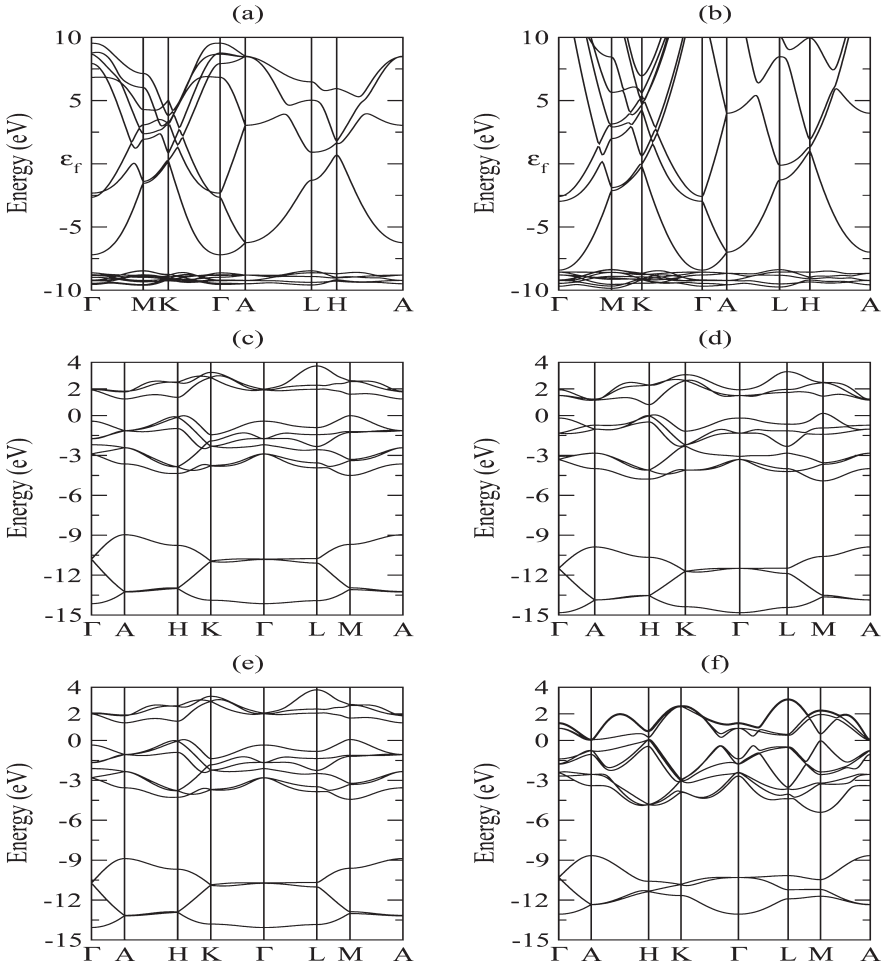

Figure 1. Electronic band structure of hcp-Cd (a, b), trigonal Se (c, d), and trigonal Te (e, f) calculated by SCC-DFTB (left panel) and PP-PBE (right panel) methods as implemented in the SIESTA package. For hcp-Cd, ε_f denotes the Fermi level for each case. For Se and Te, the zero of energy is set at the top of the valence band.

This strong wave function compression is essential in ensuring a reasonable band structure for these materials.

The electronic band structures of hcp-Cd and trigonal Se and Te obtained using the SCC-DFTB and PP-PBE methods (as implemented in SIESTA) are shown in Figure 1. From the figure, it is seen that SCC-DFTB bands are compressed in comparison to the bands obtained from DFT while retaining their shape. Such behavior is typical for the SCC-DFTB method due to the use of a minimal basis set. As a general feature, relevant states lying close to the Fermi level are reasonably described using SCC-DFTB. The trigonal Se and Te band gap (E_g) values obtained with the SCC-DFTB method (1.49 and 0.68 eV, respectively) are closer to the experimental values (1.98 and 0.33 eV, respectively) than the PP-PBE result (0.84 and 0.19 eV, respectively). It is important to mention that, usually, DFT underestimates the band gap. The good agreement for the band gap values obtained using SCC-DFTB is therefore fortuitous and due to the use of a minimum basis set. In any case, this opening of the gap using DFTB might be useful when treating systems with states lying inside the band gap.

3.2. Bulk CdO (Rock-Salt), Zinc-Blende, and Wurtzite Phase of CdS, CdSe, and CdTe. Although, the most stable phase of CdO is rock-salt, cadmium chalcogenides adopt either a zinc-blende (zb) or wurtzite (wz) crystal structure. We have calculated the bulk lattice parameters, energetics, and band structure of CdO and also of cadmium chalcogenides of both zb and wz modifications. The Brillouin-zone integration of the superstructures is calculated using the MP special k points scheme. For cadmium chalcogenides, a large number of k points and high Mesh-cutoff energies for the basis functions are used to ensure that the total energy difference between the wz and zb phases is converged to within 0.001 eV/Å. All of the structural parameters are fully relaxed to minimize the total energy.

The bulk properties of rock-salt CdO calculated by our derived SCC-DFTB parameters and PP-PBE (SIESTA) methods are given in Table 3 (top). The available experimental results[83,84] are also shown. The SCC-DFTB results for most of the bulk properties agree well with the PP-PBE as well as experimental results. However, because of the strong wave function compression used for Cd, the value of the bulk modulus shows a large deviation. Again, the difference in cohesive energy is due to overestimation of the energy calculation in DFTB method. The band structure of bulk CdO is depicted in Figure 2 together with the reference PP-PBE one. From the figure, it is seen that DFTB reproduces the shape of the bands very well.

In Table 3, we have also presented the results of bulk properties for zinc-blende phase of CdS, CdSe, and CdTe. From the table, it is clear that bulk properties calculated using our derived

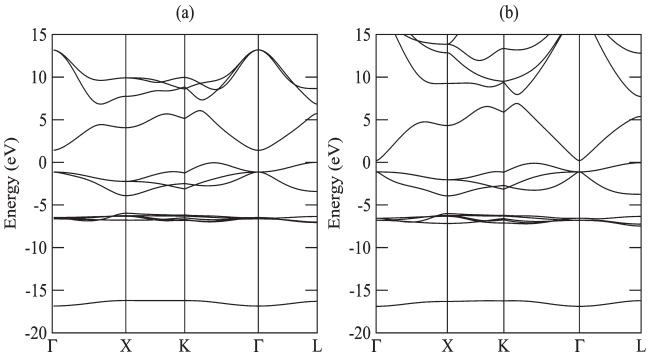

Figure 2. Electronic band structure of bulk rock-salt CdO calculated by (a) SCC-DFTB and (b) PP-PBE methods as implemented in the SIESTA package. Zero energy is set at the top of the valence band.

parameters agree well with those of PP-PBE and also experimental values.[85−87] It is important to note that, although there were large differences in the calculated and experimental bulk modulus of elemental Cd, Se, and Te, the calculated bulk modulus for the cadmium chalcogenides shows very good agreement with experimental values. The band structures of the zinc-blende phase of cadmium chalcogenides calculated with the current SCC-DFTB parameter set and with PP-PBE are shown in Figure 3. From the figure, it is seen that, although SCC-DFTB bands are little compressed, it generally reproduces the band structure features of PP-PBE. Our SCC-DFTB band gap values are higher than the corresponding PP-PBE values and are close to the experimental ones.

In our SCC-DFTB calculation, for the wurtzite structures of cadmium chalcogenides (CdX; X = S, Se, and Te), we have also varied the c/a ratios to find the minimum energy lattice parameters. Another important parameter in periodic calculation is the internal parameter u. The assumption of equal nearest-neighbor bond lengths for the wurtzite crystal leads to the ideal value

$$u = \frac{1}{3}\left(\frac{a}{c}\right)^2 + \frac{1}{4} \qquad (5)$$

In our calculation, the internal parameters u (in Å) are 0.3757, 0.3756, and 0.3754 for CdS, CdSe, and CdTe, respectively, very close to the ideal value of 0.375. This is due to the splittings of Cd-anion nearest neighbor bond lengths in the wz structure being very small. The slight decrease in the u parameter is consistent with the slight increases of the c/a ratio as the anion atomic number increases. This is because in wz semiconductors, due to the competition between bond-bending and bond-stretching forces, the c/a ratio and the u parameter always move in opposite directions. In Table 3 (bottom), we have also presented the lattice parameters and energetic properties of wurtzite cadmium chalcogenides. The SCC-DFTB lattice parameters a and c are more or less within 5% of the experimental values and very close to the PP-PBE calculations. The calculated bulk moduli using the DFTB method are in good agreement with experimental data as well as the PP-PBE method. It is observed that the bulk modulus decreases as the anion atomic number increases. At the equilibrium lattice constants, the calculated bulk moduli in the SCC-DFTB approach are 60.59, 51.02, and 38.08 GPa for the zb phase of CdS, CdSe, and CdTe, respectively. It is predicted that the bulk moduli for the wz structures are slightly smaller than their zb counterparts. The cohesive energies calculated by DFTB method

Table 3. Structural and Energetic Properties of Rock-Salt CdO and zb and wz Phases of CdS, CdSe, and CdTe Calculated Using SCC-DFTB and PP-PBE (Experimental Values Are Also Given)

	c (Å)	a (Å)	c/a	B (Gpa)	E_c (eV/atom)	E_g (eV)
			rock-salt CdO			
SCC-DFTB		4.68		168.11	8.65	2.56
PP-PBE		4.82		124.11	6.04	1.31
exptl[a]		4.70		130.10	6.08	2.38
			zb-CdS			
SCC-DFTB		5.90		61.59	7.62	3.03
PP-PBE		5.98		52.54	5.49	1.22
exptl[b]		5.83		64.30	5.56	2.55
			zb-CdSe			
SCC-DFTB		6.04		51.02	6.81	2.49
PP-PBE		6.26		44.34	5.07	0.69
exptl[b]		6.05		55.00	4.91	1.90
			zb-CdTe			
SCC-DFTB		6.46		38.08	5.83	1.91
PP-PBE		6.68		35.92	4.52	1.02
exptl[b]		6.48		44.50	4.45	1.61
			wz-CdS			
SCC-DFTB	6.80	4.17	1.63	58.71	7.62	3.04
PP-PBE	6.92	4.24	1.63	52.96	5.49	1.29
exptl[c]	6.71	4.14	1.621	62.00		2.58
			wz-CdSe			
SCC-DFTB	6.96	4.27	1.63	50.72	6.82	2.51
PP-PBE	7.22	4.43	1.63	44.37	5.07	0.75
exptl[c]	7.01	4.30	1.63	53.00		1.83
			wz-CdTe			
SCC-DFTB	7.44	4.56	1.63	37.94	5.84	1.89
PP-PBE	7.71	4.71	1.63	35.44	4.51	1.09
exptl[c]	7.45	4.55	1.637			1.60

[a] Refs 83 and 84. [b] Refs 85−87. [c] Refs 88 and 91.

are in good agreement with the PP-PBE approach and experimental ones. The electronic band structures calculated using SCC-DFTB method and PP-PBE method for the wz bulk phase of cadmium chalcogenides are shown in Figure 4. The SCC-DFTB method reproduces the PP-PBE bands very well. Our calculated band structures for both zb and wz phases of all of the chalcogenides are in good agreement with other studies available in the literature.[85,88−92] The band gap values we obtained in DFTB calculations are also close to the experimental values. Due to an incorrect description of the self-interaction in the exchange-correlation potential in the PP-PBE (or LDA), the band gaps are underestimated compared to the experimental values. With the slight differences between the zb and wz structures, the total energies, cohesive energies, and direct band gaps at the Γ point are expected to be similar for these two structures. Our SCC-DFTB calculations reproduce the energetic near-degeneracy of the two crystal structures within 5−8 MeV/Cd−X, which reflects the accuracy of the SCC-DFTB parameters.

3.3. CdX (X = S, Se, and Te) (10$\bar{1}$0) and (11$\bar{2}$0) Surfaces. The (10$\bar{1}$0) and (11$\bar{2}$0) surfaces were constructed from the

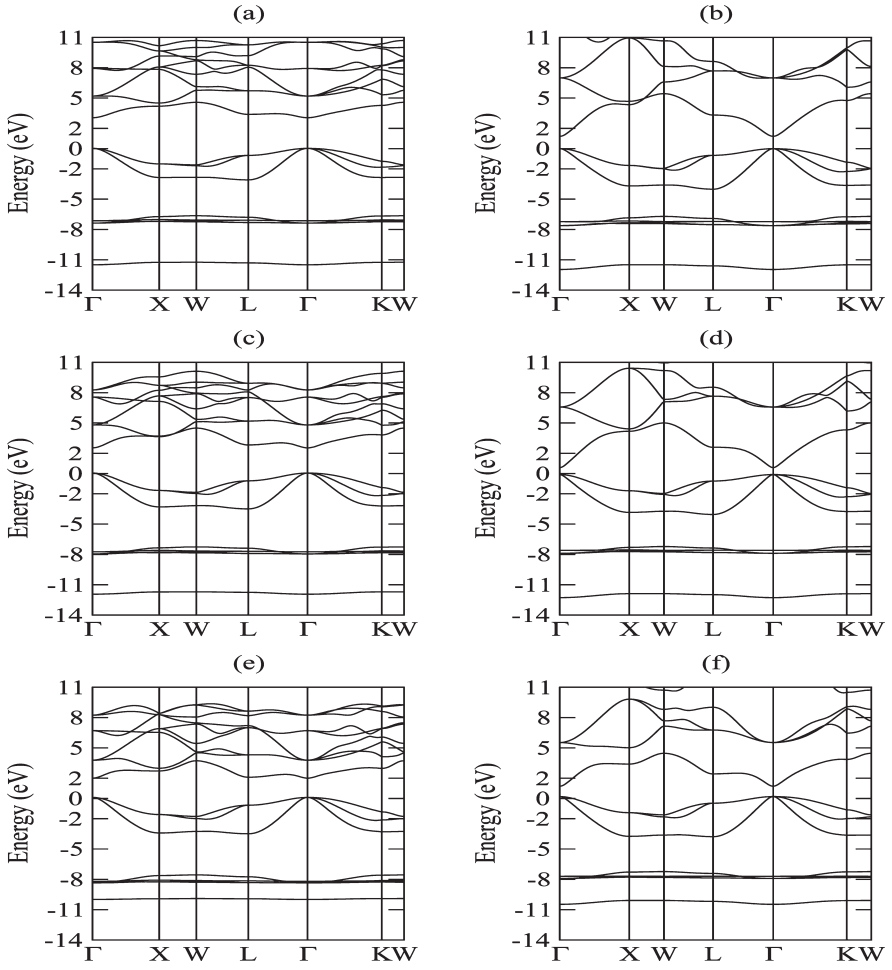

Figure 3. Electronic band structure of zb-CdS (a, b), zb-CdSe (c, d), and zb-CdTe (e, f) calculated by the SCC-DFTB (left panel) and PP-PBE (right panel) methods, as implemented in the SIESTA package. Zero energy is set at the top of the valence band for each case.

optimized bulk wz-CdX (X = S, Se, and Te) structures. The optimized side views of the hexagonal $(10\bar{1}0)$ and $(11\bar{2}0)$ surfaces of one of the representative CdX system are shown in Figure 5. The results of surface relaxation obtained from SCC-DFTB and PP-PBE for all of the chalcogenides are shown in Table 4. From the table, it is seen that the results of surface relaxation obtained through SCC-DFTB and PP-PBE results are very close to each other. The surface relaxation for all systems normally causes the chalcogen atoms to move outward while Cd atoms move inward, and this behavior is in accord with other studies.[93−98] Both the surfaces show strong surface relaxations. Thus, for $(10\bar{1}0)$ surfaces of all chalcogenides, the bond lengths d_{Cd-X} are largely shortened compared with the bulk values, while the bond lengths between the second and the third layers are little larger compared to the bulk value. For example, the Cd−S bond lengths (d_{Cd-S}) for the $(10\bar{1}0)$ surface of CdS is 2.22 Å compared to the bulk value of 2.56 Å. The Cd−S bond lengths (d'_{Cd-S}) between the second and third layers is 2.60 Å, which is slightly larger than the bulk value. The X−Cd−X angle (α) changes from the 109° bulk value to around 120° at the top surface layer for all systems, while the same angles in the inner layers (β) show very little change. However, for $(11\bar{2}0)$ surfaces of cadmium chalcogenides, Cd−X (X = S, Se, and Te) bond lengths (d_{Cd-X}) of the top surface layer shortened, and also the Cd−X (d'_{Cd-X} and d''_{Cd-X}) bond lengths between the surface and the second layer change from the bulk value. For example, Cd−S the bond length (d_{Cd-S}) in the top surface layer shortened from its bulk value of 2.56 Å to 2.45 Å, while the Cd−S lengths (d_{Cd-S} and d''_{Cd-S}) between the surface and the second layer are 2.60 Å and 2.59 Å, respectively, compared to their bulk value of 2.56 Å. However, all of the bond lengths (for both top surface layers and in the second layers) for other chalcogenides (CdSe and CdTe) shortened compared to the bulk value. The change in bond lengths Cd−X in the surface layer from the bulk values is relatively more for CdTe compared to that for CdSe and CdS. The X−Cd−X bond angles (α) at the top $(11\bar{2}0)$ surface layer increases while the Cd−X−Cd bond angles (β) decrease to a large extent from their bulk values. This contrasting behavior in the bond angle values is due to the inward movement of Cd atoms and outward movement of chalcogen atoms. However, in the inner layer, these angles remain almost the same as those of bulk values. The universal character of the surface atomic geometries for each cleavage surface was also obtained by Duke and Wang.[93−96] The prediction of the surface relaxation of cadmium chalcogenides is similar to the results of a low-energy electron diffraction (LEED) study of related semiconductor ZnO.[97] The surface energies of both $(10\bar{1}0)$ and $(11\bar{2}0)$ surfaces of all of the chalcogenides calculated by SCC-DFTB and PP-PBE methods are also shown in Table 4. As expected, the SCC-DFTB method overestimates the surface energies compared to the

dx.doi.org/10.1021/ct200266f |J. Chem. Theory Comput. 2011, 7, 2262–2276

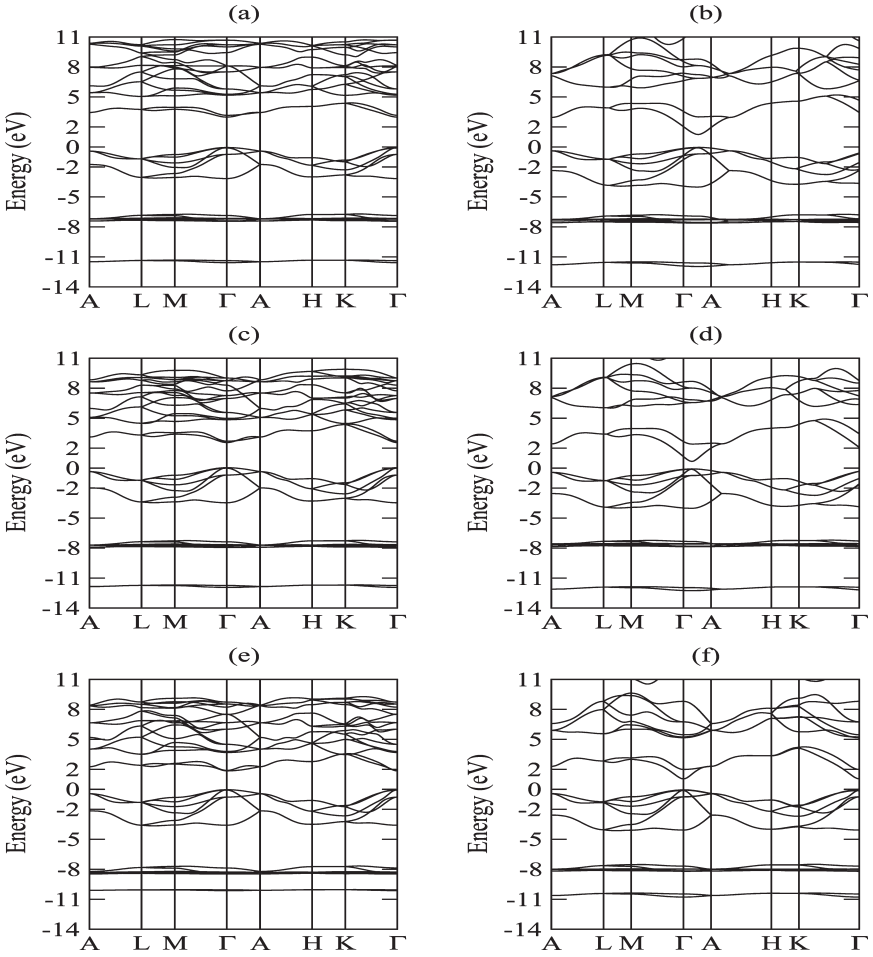

Figure 4. Electronic band structure of wz-CdS (a, b), wz-CdSe (c, d), and wz-CdTe (e, f) calculated by SCC-DFTB (left panel) and PP-PBE (right panel) methods as implemented in SIESTA package. Zero energy is set at the top of the valence band for each case.

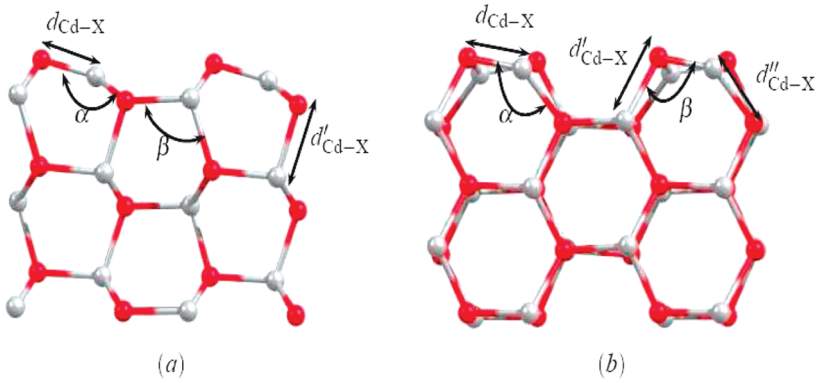

Figure 5. Optimized structure of representative CdX (a) $(10\bar{1}0)$ and (b) $(11\bar{2}0)$ surfaces (side view).

PP-PBE method. The calculated surface energies are in excellent agreement with the very recent study of Li et al.[98] The surface energy of CdX decreases as X changes from S to Te. The surface energy of all of these systems suggests that $(10\bar{1}0)$ surfaces are relatively more stable compared to corresponding $(11\bar{2}0)$ surfaces. In Figures 6 and 7, we have shown the band structures of $(10\bar{1}0)$ and $(11\bar{2}0)$ surfaces, respectively, calculated by both SCC-DFTB and PP-PBE methods. As is evident from the figures, the SCC-DFTB band dispersion agrees very well with those of PP-PBE. As expected, the calculated SCC-DFTB band gap values in all cases are higher than the corresponding PP-PBE values. Our calculated band structure of $(10\bar{1}0)$ surfaces of CdS and CdSe are also in good agreement with those studied by Duke and Wang.[93−96]

3.4. CdX (X = S, Se, and Te) $(10\bar{1}0)$ and $(11\bar{2}0)$ Faceted Hexagonal Nanowires. Semiconductor nanowires have been the subject of intense investigation because of their diverse application in the field of nanotechnology.[15,16] So, for further

validation of SCC-DFTB parametrization, we investigated $(10\bar{1}0)$ and $(11\bar{2}0)$ faceted hexagonal nanowires for all cadmium chacogenides. In Figure 8, we have shown the optimized cross sections of one of the representative $(10\bar{1}0)$ and $(11\bar{2}0)$ faceted hexagonal nanowires of one chalcogenide. All of the nanowires follow a similar relaxation in the surface layers to that of the corresponding $(10\bar{1}0)$ and $(11\bar{2}0)$ surfaces. Thus, the surface cadmium atoms move relatively inward while the chalcogenides move outward. In Table 5, we have presented the details of the surface relaxation calculated using both the SCC-DFTB and PP-PBE methods of all $(10\bar{1}0)$ and $(11\bar{2}0)$) faceted CdX nanowires. As is found for surfaces, the Cd−X bond lengths ($d_{\mathrm{Cd-X}}$) for $(10\bar{1}0)$ faceted nanowires are shortened compared with their bulk values. However, the change in Cd−X bond lengths ($d'_{\mathrm{Cd-X}}$) between the second and third layers is very small for CdS, while those of CdSe and CdTe are shortened compared to their bulk values. This is in contrast to the behavior of the corresponding surfaces where the bond lengths were expanded compared to their bulk values. The X−Cd−X angles of both the top surface layer (α) and the inner layer (β) for all systems show a large deviation from the bulk value (109°). The results of surface relaxation of the $(11\bar{2}0)$ surfaces are very much similar to those of the corresponding surfaces. In the table, we have also presented the value of the formation energy of the nanowires. The formation energy (E_f) of a given nanowire is defined by

$$E_f = \left(\frac{E_{NW}}{n} - \frac{E_{bulk}}{2}\right) \quad (6)$$

Table 4. Calculated Geometry (Bond Lengths Are in Å and Bond Angles Are in deg) and Surface Energy γ (in J/m^2) of Both $(10\bar{1}0)$ and $(11\bar{2}0)$ Surfaces of Cadmium Chalcogenides

	$(10\bar{1}0)$					$(11\bar{2}0)$					
	$d_{\mathrm{Cd-X}}$	$d'_{\mathrm{Cd-X}}$	α	β	γ	$d_{\mathrm{Cd-X}}$	$d'_{\mathrm{Cd-X}}$	$d''_{\mathrm{Cd-X}}$	α	β	γ
CdS											
SCC-DFTB	2.22	2.60	122	107	0.59	2.45	2.60	2.59	113	97	0.63
PP-PBE	2.46	2.62	123	104	0.35	2.50	2.56	2.57	120	92	0.34
CdSe											
SCC-DFTB	2.38	2.71	121	104	0.39	2.45	2.58	2.57	117	97	0.40
PP-PBE	2.59	2.74	124	102	0.34	2.64	2.68	2.69	121	90	0.28
CdTe											
SCC-DFTB	2.55	2.94	121	102	0.22	2.61	2.68	2.68	118	96	0.23
PP-PBE	2.77	2.90	125	103	0.21	2.82	2.85	2.86	122	88	0.21

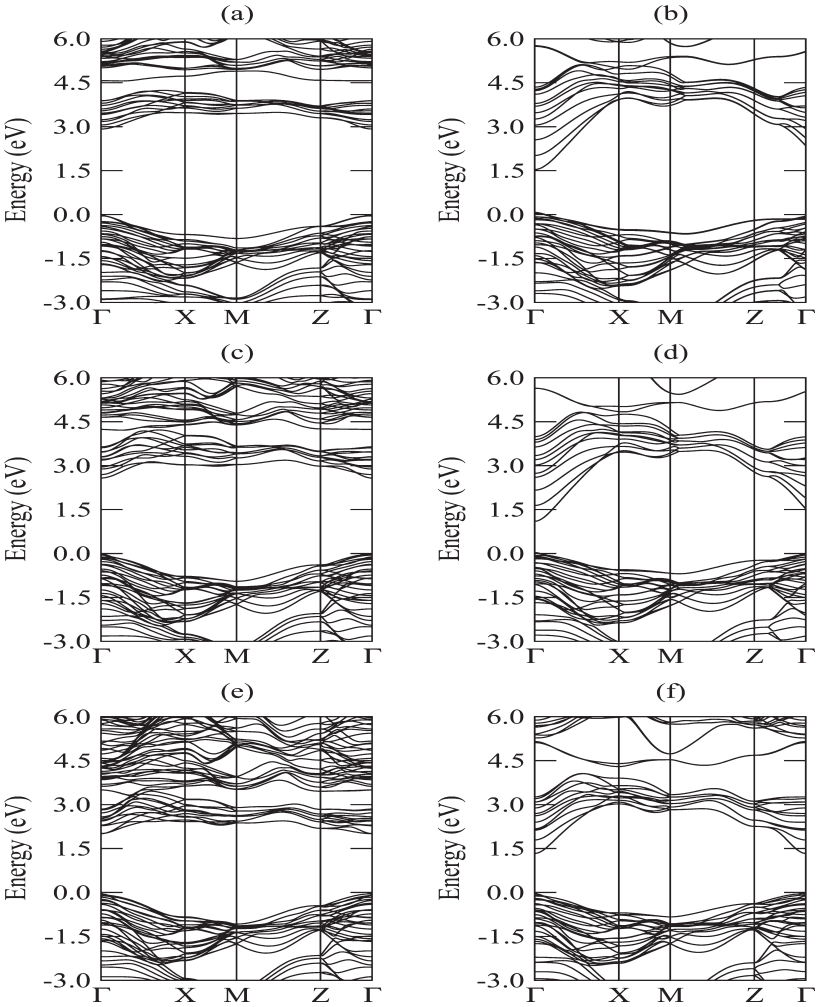

Figure 6. Electronic band structures of CdX [X = S (a, b), Se (c, d), and Te (e, f)] $(10\bar{1}0)$ surfaces, calculated with SCC-DFTB (left panel) and PP-PBE (right panel) methods, as implemented in the SIESTA package. Zero energy is set at the top of the valence band for each case.

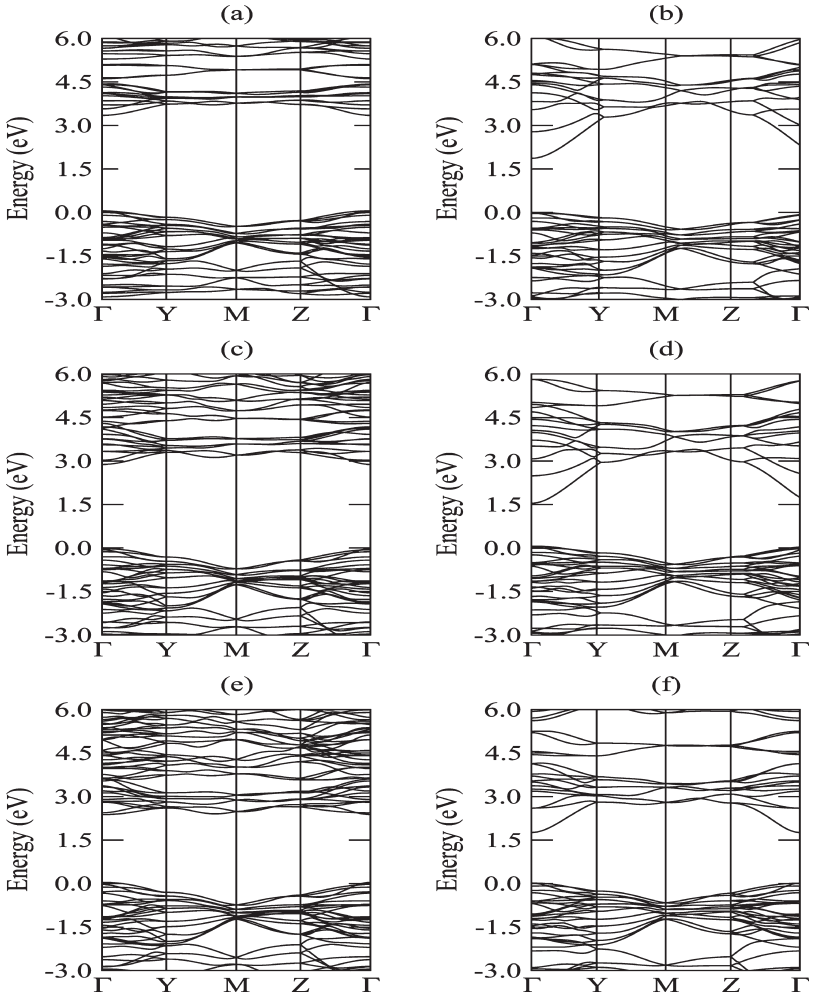

Figure 7. Electronic band structures of CdX [X = S (a, b), Se (c, d), and Te (e, f)] $(11\bar{2}0)$ surfaces, calculated with SCC-DFTB (left panel) and PP-PBE (right panel) methods, as implemented in the SIESTA package. Zero energy is set at the top of the valence band for each case.

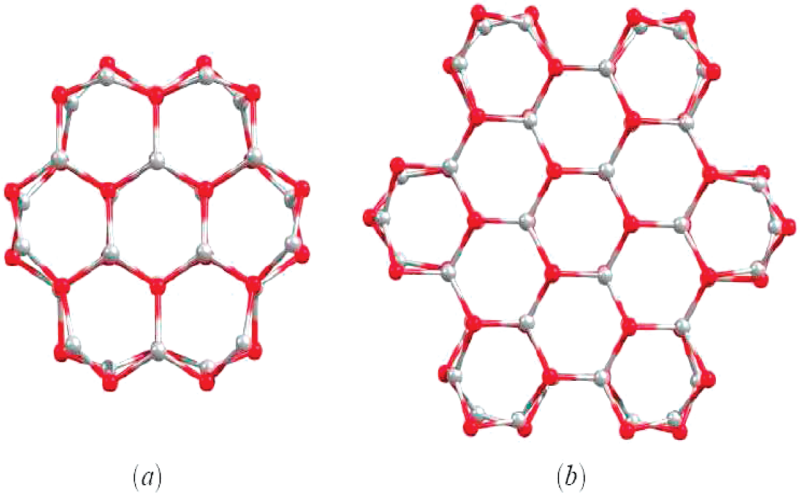

Figure 8. Optimized structure of representative CdX (a) $(10\bar{1}0)$ and (b) $(11\bar{2}0)$ nanowires (top view).

where E_{NW} is the total energy of the nanowire, n is the total number of Cd−X units in the CdX nanowire, and E_{bulk} is the energy of the bulk wz-CdX. From the values of the formation energy, we can infer that $(10\bar{1}0)$ faceted nanowires are relatively more stable compared to $(11\bar{2}0)$ faceted nanowires, although the differences in formation energy of these two forms of nanowire

are very small. As expected, the value of the formation energy of both $(10\bar{1}0)$ and $(11\bar{2}0)$ faceted nanowires decreases from CdS to CdTe. In most of the cases, our SCC-DFTB results are close to the corresponding PP-PBE results. In Figure 9, we have shown the band structure of $(10\bar{1}0)$ faceted nanowires of CdX (X = S, Se, and Te) respectively calculated with both SCC-DFTB and PP-PBE methods. In Figure 10, we have shown the same for $(11\bar{2}0)$ faceted nanowires. As is evident from the figures, SCC-DFTB reproduces all of the important bands very well. Because of the use of a minimal basis set, the conduction bands show little deviation from PP-PBE results. The other feature is that the SCC-DFTB bands are relatively more compressed compared to PP-PBE bands. The bands of all studied nanowires are more localized compared to the corresponding surfaces. Our calculated SCC-DFTB electronic band structures are also similar to that obtained by Huang et al.[99] The band gap values obtained by using the SCC-DFTB method are higher than those of the PP-PBE method. As mentioned earlier, this is due to the fact that the SCC-DFTB method generally overestimates this property. Interestingly, the band gap values of studied nanowires are larger compared to their bulk values, consistent with the quantum confinement effects. There are experimental studies on CdS and CdSe nanowires with diameters of around 70−100 nm, and their band gap values are almost close to bulk band gap values.[100,101] So, nanowires of smaller diameters will show a quantum confinement effect and correspondingly have higher band gap values. Huang et al. also reported similar band gap behavior in their recent study on CdS and CdSe NWs.[99] The SCC-DFTB prediction of the stability order of these nanowires also is the same as that of PP-PBE results.

Table 5. Calculated Geometry (Bond Lengths Are in Å and Bond Angles Are in deg) and Formation Energy E_f (in eV/pair) of Both $(10\bar{1}0)$ and $(11\bar{2}0)$ Nanowires of Cadmium Chalcogenides

	$(10\bar{1}0)$					$(11\bar{2}0)$					
	d_{Cd-X}	d'_{Cd-X}	α	β	E_f	d_{Cd-X}	d'_{Cd-X}	d''_{Cd-X}	α	β	E_f
						CdS					
SCC-DFTB	2.29	2.57	124	118	0.48	2.53	2.58	2.54	111	96	0.42
PP-PBE	2.49	2.55	120	118	0.27	2.52	2.56	2.53	116	91	0.24
						CdSe					
SCC-DFTB	2.44	2.55	122	119	0.32	2.48	2.57	2.50	116	96	0.29
PP-PBE	2.63	2.68	120	119	0.24	2.65	2.68	2.65	118	89	0.21
						CdTe					
SCC-DFTB	2.60	2.66	121	120	0.20	2.64	2.68	2.65	116	95	0.19
PP-PBE	2.81	2.86	120	120	0.21	2.83	2.86	2.83	118	87	0.18

3.5. Small Molecular Systems. Finally, we have tested the transferability of our derived SCC-DFTB parameters with respect to DFT by calculating the structural and energetic

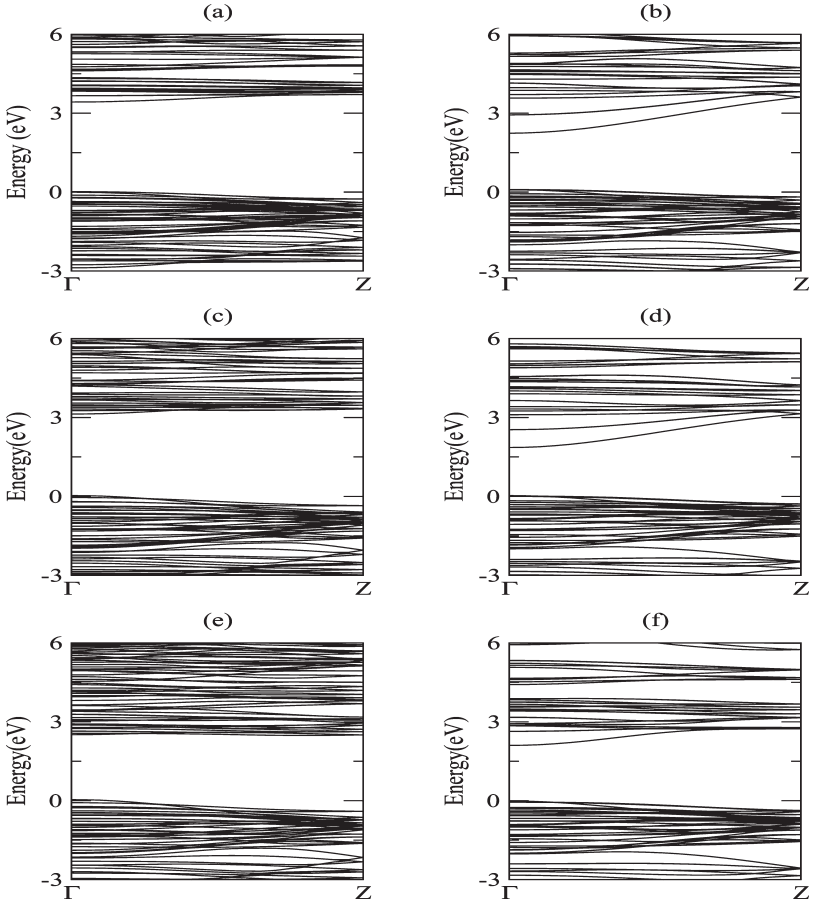

Figure 9. Electronic band structure of $(10\bar{1}0)$ faceted nanowires for CdS (a, b), CdSe (c, d), and CdTe (e, f) calculated with the SCC-DFTB (left panel) and PP-PBE (right panel) methods, as implemented in the SIESTA package. Zero energy is set at the top of the valence band for each case.

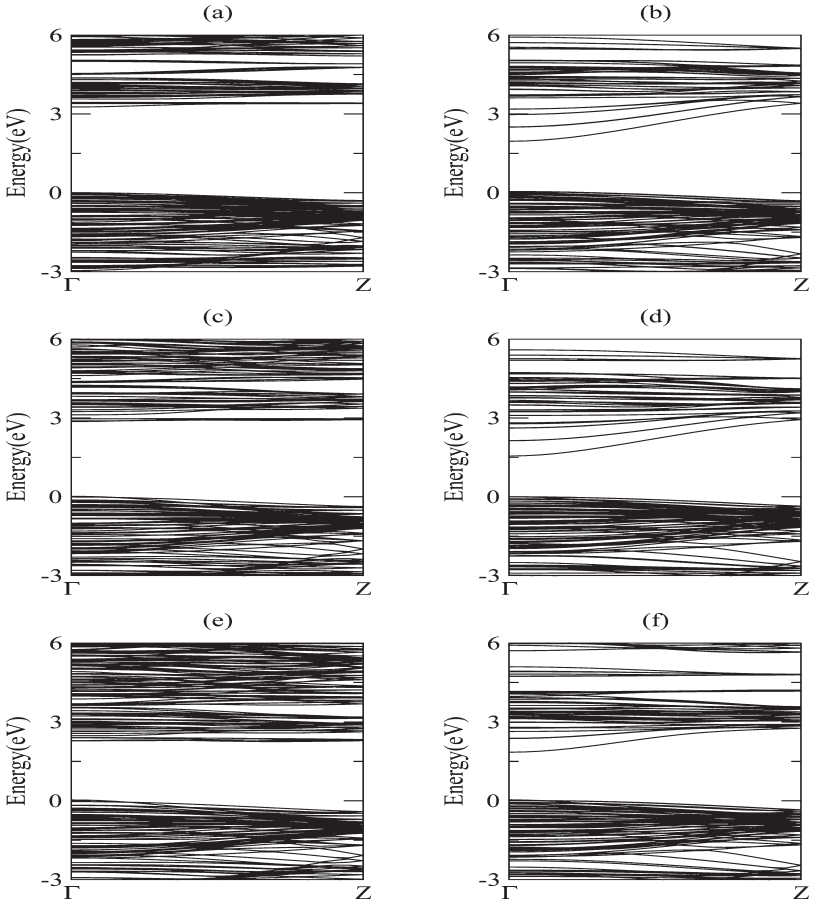

Figure 10. Electronic band structure of $(11\bar{2}0)$ faceted nanowires for CdS (a, b), CdSe (c, d), and CdTe (e, f) calculated with the SCC-DFTB (left panel) and PP-PBE (right panel) methods, as implemented in the SIESTA package. Zero energy is set at the top of the valence band for each case.

Table 6. Atomic-Spin-Dependent Constants $W_{All'}$ of Se and Te (in au)

$W_{All'}$			Se			Te		
W_{ss}	W_{sp}	W_{sd}	−0.018	−0.014	−0.000	−0.014	−0.011	−0.000
W_{p}	W_{pp}	W_{pd}	−0.014	−0.014	−0.000	−0.011	−0.011	−0.000
W_{ds}	W_{dp}	W_{dd}	−0.000	−0.000	−0.096	−0.000	−0.000	−0.083

properties of some simple diatomic molecules and small molecular systems. As all systems studied so far are closed-shell systems, we used the nonspin polarized SCC-DFTB method. However, for diatomic molecules, we have used the spin-polarized SCC-DFTB method of Köhler et al.[102] The atomic-spin-dependent constants $W_{All'}$ needed for the spin-polarized SCC-DFTB method are calculated by taking the second derivatives of the total atomic energy with respect to the spin density; at the point where the spin density is zero, this derivative reduces to

$$W_{All'} = \frac{1}{2}\left(\frac{\partial \varepsilon_{Al}^{\uparrow}}{\partial n_{l}^{\uparrow}} - \frac{\partial \varepsilon_{Al}^{\uparrow}}{\partial n_{l}^{\downarrow}}\right)_{\rho=0} = W_{Al'l} \qquad (7)$$

where n_l and $n_{l'}$ are the occupation numbers of atomic shells l and l', respectively, and $\varepsilon_{Al}^{\uparrow}$ is the atomic Kohn−Sham orbital energy for alpha ($\uparrow$) spin. The second derivative values are computed

Table 7. Comparison between SCC-DFTB, PP-PBE, and B3LYP Results on the Binding Energy (in eV) and Equilibrium Bond Length (in Å) of Simple Diatomic Molecules[a]

	dimer	SCC-DFTB		PP-PBE		B3LYP/SBK+6-31G(d,p)	
	A−B	E_b	r	E_b	r	E_b	r
d	Cd−H	0.86	1.93	0.86	1.86	0.82	1.85
t	Cd−C	2.48	2.16	1.54	2.19	2.66	2.23
q	Cd−N	1.67	2.22	0.44	2.39	2.97	2.48
s	Cd−O	3.15	1.89	1.21	1.94	3.21	1.92
d	Se−H	3.15	1.51	3.08	1.51	3.71	1.49
s	Se−C	6.70	1.71	6.44	1.71	8.89	1.69
d	Se−N	5.48	1.71	3.89	1.70	7.42	1.69
t	Se−O	4.95	1.72	4.52	1.71	4.17	1.70
t	Se−S	3.92	2.05	3.98	2.10	3.48	2.11
d	Te−H	2.84	1.70	2.67	1.72	3.12	1.68
s	Te−C	5.10	1.94	5.05	1.95	7.16	1.92
d	Te−N	3.70	1.93	2.81	1.95	6.47	1.91
t	Te−O	4.35	1.95	3.86	1.94	3.62	1.87
t	Te−S	3.77	2.33	3.54	2.32	3.94	2.31
t	Te−Se	3.16	2.50	3.16	2.49	3.38	2.49

[a] s, d, t, and q denote singlet, doublet, triplet, and quartet spin states, respectively.

dx.doi.org/10.1021/ct200266f |J. Chem. Theory Comput. 2011, 7, 2262–2276

using the finite difference method. We here only calculated the values of atomic spin constants $W_{All'}$ for Se and Te, and they are given in Table 6. In case of the Cd atom, it is not required due to the closed-shell nature of it. For all other atoms like H, C, N, O, and S, we have used the spin constants calculated previously.[102]

The binding energies and equilibrium bond lengths calculated by the SCC-DFTB method, PP-PBE method, and also B3LYP/SBK+6-31G(d,p) of several diatomic systems are shown in Table 7. The SCC-DFTB results in most of the cases are very promising. Experimental results for some diatomic molecules are also available, and we have compared our theoretical results with these. For example, CdH is known to have an experimental binding energy of 0.71 eV and an equilibrium bond length of 1.86 Å.[103] Our calculated binding energy (0.86 eV) and bond length (1.93 Å) are close to experimental values. The ground state of the CdC molecule is a triplet, and the experimental binding energy and bond length are 1.91 eV and 2.17 Å, respectively.[104] Our SCC-DFTB calculation predicts the binding energy to be 2.48 eV, slightly overestimated, but it predicts the bond length (2.16 Å) more accurately (within 0.01 Å). The bond length of the diatomic molecule CdO in its singlet ground state calculated by the SCC-DFTB method (1.90 Å) also agrees well with the experimental value of 1.90 Å.[105] In the cases of Se−B (B = O and S) and Te−B (B = O, S and Se), the bond lengths increase while the binding energies decrease with an increasing size of B. This fact is in good agreement with the other DFT calculations and also with the experimental results.[104,106]

Table 8. Comparison between SCC-DFTB, SIESTA (PP-PBE), G03 (B3LYP), and Experimental Results on the Binding Energy (in eV) and Equilibrium Bond Angle (in deg) and Length (in Å) of AB_2-Type Molecules[a]

	SCC-DFTB			PP-PBE			B3LYP/-SBK+6-31G-(d,p)			Exp.		
Molecule												
AB_2	E_b	θ	r	E_b	θ	r	E_b	θ	r	E_b	θ	r
CdH_2	3.88	180	1.76	4.23	180	1.71	4.10	180	1.75	3.06	180	1.75[b]
SeH_2	3.36	97	1.50	3.17	90	1.51	4.05	91	1.48	3.42	91.5	1.48[c]
SeO_2	5.00	115	1.71	3.97	111	1.69	3.87	112.7	1.65	4.37	114	1.61[d]
SeS_2	3.45	119	2.09	3.05	115	2.13	2.81	115	2.14			
TeH_2	2.98	95	1.70	2.77	89	1.71	3.55	89.6	1.68	2.82	90	1.69[e]
TeO_2	4.49	116	1.93	3.43	109	1.92	3.67	111.5	1.81	3.37	102	1.90[f]
TeS_2	3.57	117	2.34	2.88	112	2.33	2.65	113	2.31		103.4	2.39[g]
$TeSe_2$	2.88	118	2.52	2.50	113	2.52	3.07	113	2.51			2.50[g]

[a] All molecules have been calculated in the singlet state. [b] Ref 107. [c] Refs 108 and 109. [d] Ref 110. [e] Ref 106. [f] Refs 104 and 110. [g] Ref 104.

In Table 8, we presented our results on AB_2 types of molecules. The equilibrium bond lengths of several systems calculated by SCC-DFTB are close to the PP-PBE and B3LYP/SBK+6-31G(d,p) results. However, the bond angles are larger than the corresponding DFT values. As an illustrative example, we consider the CdH_2 molecule. The CdH_2 molecule in its singlet ground state is known experimentally to have a bond length of 1.75 Å and a bond angle of 180° from infrared spectroscopy of the matrix isolated molecule.[107] The equilibrium bond length and bond angle calculated by SCC-DFTB parametrization reproduces these geometrical features very well, and they are also close to the values obtained from PP-PBE and B3LYP/SBK+6-31G(d,p) calculations. The good agreement among SCC-DFTB, PP-PBE,

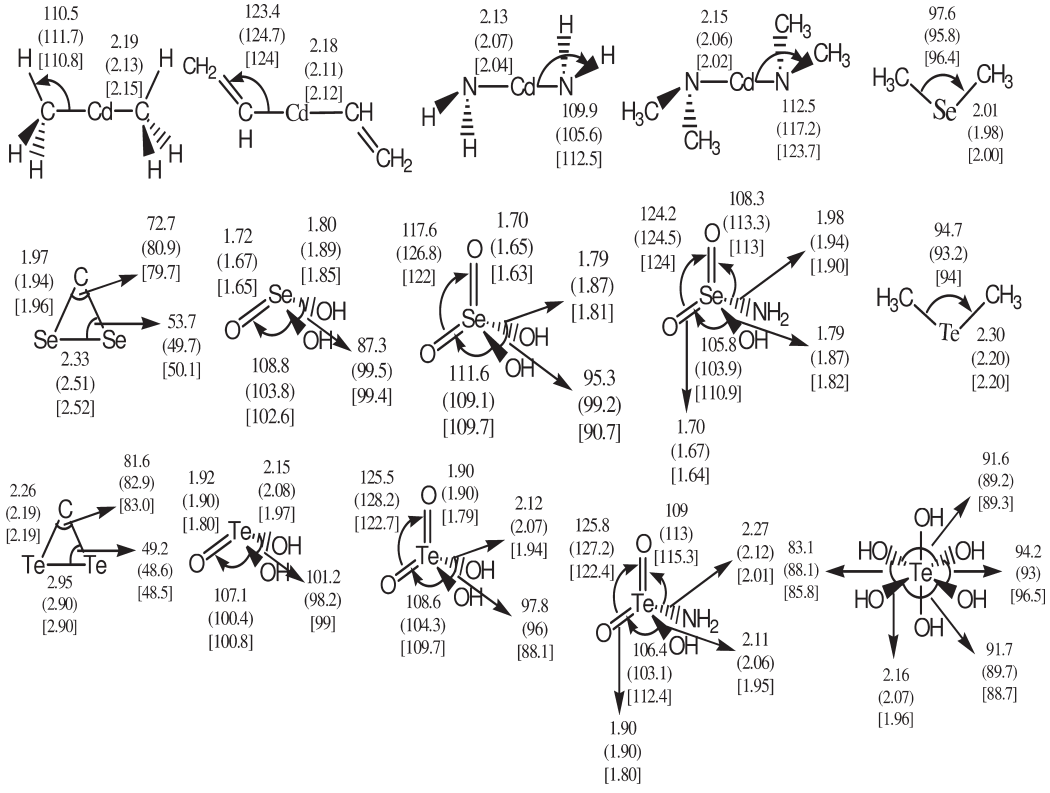

Figure 11. Schematic view of a few small molecules together with their equilibrium geometric parameters obtained with SCC-DFTB (without brackets), PP-PBE in parentheses, and B3LYP/SBK+6-31G(d,p) in brackets. The bond lengths are in Å and angles are in deg.

dx.doi.org/10.1021/ct200266f |J. Chem. Theory Comput. 2011, 7, 2262–2276

B3LYP/SBK+6-31G(d,p), and experimental[108−111] results on bond lengths, bond angles, and binding energies (with usual DFTB overestimation) of several AB_2 type molecules, as presented in Table 8, makes us believe that the derived parameters are highly transferable, and one can study either the adsorption of small molecules on the cadmium chalcogenide surfaces or different types of surface passivation effects.

In addition, we have calculated the geometric features of several model molecules with SCC-DFTB and PP-PBE and also with B3LYP/SBK+6-31G(d,p). The results are shown in Figure 11. The bond lengths and bond angles of several model molecules calculated using the SCC-DFTB method are very close to the other DFT calculations. The binding energyies per bond are also in good agreement with those of PP-PBE and B3LYP/SBK+6-31G(d,p) calculations. The experimental results of a few molecules studied here are also available in the literature. Thus, the experimental Cd−C bond length in $Cd(CH_3)_2$ is 2.21 Å. The bond length obtained with the SCC-DFTB method is very close to the experimental value.[112] The experimental bond length and bond angle of $Se(CH_3)_2$ are found to be 1.98 Å and 98°, respectively.[113,114] These values are also in very good agreement with our SCC-DFTB values.

4. CONCLUSION

A complete SCC-DFTB parametrization for cadmium and its interaction with oxygen, carbon, hydrogen, sulfur, selenium, tellurium, etc. has been developed in order to get the best possible description of periodic and molecular systems involving these elements. Using this parameter set, we have calculated the bulk properties (*i.e.*, lattice constants, bulk moduli, cohesive energies, band structures, etc.) of hcp-Cd, trigonal Se and Te, rock-salt CdO, and zb and wz cadmium chalcogenides (CdS, CdSe, CdTe). Our calculated values are in good agreement with the reference DFT calculations and also with experimental results. We have also checked the transferability of SCC-DFTB parameters by calculating the electronic structure of several nanostructures such as surfaces and nanowires. Finally, we have tested the transferability of our SCC-DFTB parameters by calculating the structural and energetic properties of some simple diatomic molecules and small molecular systems. The real world application of semiconductor nanoparticles requires the integration of smaller nanoparticles and 1-d nanostructures to form large nanostructures. However, to date, theoretical studies in this particular field are restricted to only isolated nanoparticles and 1-d nanotubes or wires. This is primarily because of the unavailability of appropriate methods to handle nanostructures composed of a large number of atoms. We do hope that, with the derived SCC-DFTB parameter of the cadmium chalcogenides set and taking advantage of the computational efficiency of the SCC-DFTB method, one may be able to study large nanostructures of cadmium chalcogenides.

AUTHOR INFORMATION

Corresponding Author

*E-mail: pranab.sarkar@visva-bharati.ac.in.

ACKNOWLEDGMENT

The financial support from DST, New Delhi [SR/NM/NS-49/2007] and UGC, New Delhi, through research grants are gratefully acknowledged. S.S. is grateful to CSIR, New Delhi for the award of a Junior Research Fellowship (JRF). A.L.R. acknowledges the German Science Foundation under the grants SPP-1165 and DIP-40100474.

REFERENCES

(1) Heath, J. R.; Shiang, J. J. *Chem. Soc. Rev.* **1998**, *27*, 65–71.
(2) Bruchez, M.; Morronne, M.; Gin, P.; Weiss, S.; Alivisatos, A. P. *Science* **1998**, *281*, 2013–2016.
(3) Alivisatos, A. P. *Science* **1996**, *271*, 933–937.
(4) Hoffman, M. R.; Martin, S. T.; Choi, W.; Bahnemann, D. W. *Chem. Rev.* **1995**, *95*, 69–96.
(5) Burda, C.; Chen, X.; Narayanan, R.; El-Sayed, M. A. *Chem. Rev.* **2005**, *105*, 1025–102.
(6) Fu, X.; Peng, Z.-J.; Li, D.; Zhang, L.; Xiao, J.-Y.; Fang, Z.-Y. *Nanotechnology* **2011**, *22*, 175601.
(7) Pan, H.; Poh, C. K.; Zhu, Y.; Xing, G.; Chin, K. C.; Feng, Y. P.; Lin, J.; Sow, C. H.; Ji, W.; Wee, A. T. S. *J. Phys. Chem. C* **2008**, *112*, 11227.
(8) Willner, I.; Willner, B. *Pure Appl. Chem.* **2002**, *74*, 1773–1783.
(9) Nisman, R.; Dellaire, G.; Ren, Y.; Li, R.; Bazett-Jones, D. P. *J. Histochem. Cytochem.* **2004**, *52*, 13.
(10) Mansson, A.; Sundberg, M.; Balaz, M.; Bunk, R.; Nicholls, I. A.; Omling, P.; Tagerud, S.; Montelius, L. *Biochem. Biophys. Res. Commun.* **2004**, *314*, 529.
(11) Nishiuchi, K.; et al. *Jpn. J. Appl. Phys.* **1998**, *37*, 2163.
(12) Klein, D. L.; Roth, R.; Lim, A. K. L.; Alivisatos, A. P.; McEuen, P. L. *Nature* **1997**, *389*, 699.
(13) Hu, J.; Li, L.-S.; Yang, W.; Manna, L.; Wang, L.-W.; Alivisatos, A. P. *Science* **2001**, *292*, 2060.
(14) Murray, C. B.; Kagan, C. R.; Bawendi, M. G. *Science* **1995**, *270*, 1335.
(15) Cui, Y.; Wei, Q. Q.; Park, H. K.; Lieber, C. M. *Science* **2001**, *293*, 1289.
(16) Wang, D. M.; Song, J.; Mu, Y.; Lieber, C. M. *Nano Lett.* **2003**, *3*, 1255.
(17) Wang, G. X.; Park, M. S.; Liu, H. K.; Wexler, D.; Chen, J. *Appl. Phys. Lett.* **2006**, *88*, 193115.
(18) Colvin, V. L.; Schlamp, M. C.; Alivisatos, A. P. *Nature* **1994**, *370*, 354–357.
(19) Radloff, C.; Moran, C. E.; Jackson, J. B.; Halas, N. *J. Mol. Nanoelectron.* **2003**, 229–262.
(20) Yu, A. M.; Meiser, F.; Cassagneau, T.; Caruso, F. *Nano Lett.* **2004**, *4*, 177.
(21) Pinaud, F.; King, D.; Moore, H. P.; Weiss, S. *J. Am. Chem. Soc.* **2004**, *126*, 6115.
(22) Sukhanova, A.; Devy, M.; Venteo, L.; Kaplan, H.; Artemyev, M.; Oleinikov, V.; Klinov, D.; Pluot, M.; Cohen, J. H. M.; Nabiev, I. *Anal. Biochem.* **2004**, *324*, 60.
(23) Derfus, A. M.; Chan, W. C. W.; Bhatia, S. N. *Nano Lett.* **2004**, *4*, 11.
(24) Wang, L. -W.; Zunger, A. *Phys. Rev. B* **1996**, *53*, 9579.
(25) Mizel, A.; Cohen, M. L. *Phys. Rev. B* **1997**, *56*, 6737.
(26) Eichkorn, K.; Ahlrichs, R. *Chem. Phys. Lett.* **1998**, *288*, 235.
(27) Ramkrishna, M. V.; Friesner, R. A. *J. Chem. Phys.* **1991**, *95*, 8309.
(28) Hill, N. A.; Whaley, K. B. *J. Chem. Phys.* **1994**, *100*, 2831.
(29) Tomasulo, A.; Ramkrishna, M. V. *J. Chem. Phys.* **1996**, *105*, 3612.
(30) Wang, L.-W.; Zunger, A. *J. Phys. Chem. B* **1998**, *102*, 6449.
(31) Leung, K.; Pokrant, S.; Whaley, K. B. *Phys. Rev. B* **1998**, *57*, 12291.
(32) Pokrant, S.; Whaley, K. B. *Eur. Phys. J. D* **1999**, *6*, 255.
(33) Troparevsky, M. C.; Chelikowsky, J. R. *J. Chem. Phys.* **2001**, *114*, 943.
(34) Deglmann, P.; Ahlrichs, R.; Tsereteli, K. *J. Chem. Phys.* **2002**, *118*, 1585.

(35) Joswig, J.-O.; Springborg, M.; Seifert, G. *J. Phys. Chem.* **2000**, *104*, 2617.
(36) Sarkar, P.; Springborg, M. *Phys. Rev. B* **2003**, *68*, 235409.
(37) Spano, E.; Hamad, S.; Catlow, C. R. *J. Phys. Chem. B* **2003**, *107*, 10337.
(38) Hamad, S.; Catlow, C. R.; Spano, E.; Matxain, J. M.; Ugalde, J. M. *J. Phys. Chem. B* **2005**, *109*, 2703.
(39) Sapra, S.; Sarma, D. D. *Phys. Rev. B* **2004**, *69*, 125304.
(40) Drager, E. W.; Grossman, J. C.; Williamson, A. J.; Galli, G. *Phys. Rev. Lett.* **2003**, *90*, 167402.
(41) Drager, E. W.; Grossman, J. C.; Williamson, A. J.; Galli, G. *J. Chem. Phys.* **2003**, *120*, 10807.
(42) Huang, X.; Lindgren, E.; Chelikowsky, J. R. *Phys. Rev. B* **2005**, *71*, 165328.
(43) Roy, S.; Springborg, M. *J. Phys. Chem. A* **2005**, *109*, 1324.
(44) Pal, S.; Goswami, B.; Sarkar, P. *J. Chem. Phys.* **2005**, *123*, 044311.
(45) Goswami, B.; Pal, S.; Sarkar, P.; Seifert, G.; Springborg, M. *Phys. Rev. B* **2006**, *73*, 205312.
(46) Joswig, J.-O.; Seifert, G.; Niehaus, T. A.; Springborg, M. *J. Phys. Chem. B* **2003**, *107*, 2897.
(47) Pal, S.; Sharma, R.; Goswami, B.; Sarkar, P.; Bhattacharyya, S. P. *J. Chem. Phys.* **2009**, *130*, 214703.
(48) Rogach, A. L.; Franzl, T.; Klar, T. A.; Feldmann, J.; Gaponik, N.; Lesnyak, V.; Shavel, A.; Eychmüller, A.; Rakovich, Y. P.; Donegan, J. F. *J. Phys. Chem. C* **2007**, *111*, 14628.
(49) Kamat, P. V. *J. Phys. Chem. C* **2007**, *111*, 2834.
(50) Plass, R.; Pelet, S.; Krueger, J.; Gratzel, M.; Bach, U. *J. Phys. Chem. B* **2002**, *106*, 7578–7580.
(51) Peng, X. G.; Manna, L.; Yang, W. D.; Wickham, J.; Scher, E.; Kadavanich, A.; Alivisatos, A. *Nature* **2000**, *404*, 59–63.
(52) Tang, K.; Qian, Y.; Zeng, Z.; Yang, X. *Adv. Mater.* **2003**, *15*, 448–450.
(53) Liu, Y.; Xu, Y.; Li, J.-P.; Zhang, B.; Wu, D.; Sun, Y.-H. *Chem. Mater.* **2004**, *33*, 1162–1163.
(54) Ma, C.; Ding, Y.; Moore, D.; Wang, X.; Wang, Z. L. *J. Am. Chem. Soc.* **2004**, *126*, 708–709.
(55) Korgel, B. A.; Monbouquette, H. G. *Langmuir* **2000**, *16*, 3588–3594.
(56) Petrov, D. V.; Santos, B. S.; Pereira, G. A. L.; Donegat', C. D. M. *J. Phys. Chem. B* **2002**, *106*, 5325–5334.
(57) Zhong, X.; Liu, S.; Zhang, Z.; Li, L.; Wei, Z.; Knoll, W. *J. Mater. Chem.* **2004**, 2790–2794.
(58) Zhong, X.; Han, M.; Dong, Z.; White, T. J.; Knoll, W. *J. Am. Chem. Soc.* **2003**, *125*, 8589–8594.
(59) Zhong, X.; Zhang, Z.; Liu, S.; Han, M.; Knoll, W. *J. Phys. Chem. B* **2004**, *108*, 15552–15559.
(60) Rakovich, Y. P.; Volkov, Y.; Sapra, S.; Susha., A. S.; Döblinger, M.; Donegan, J. F.; Rogach, A. L. *J. Phys. Chem. C* **2007**, *111*, 18927.
(61) Corrigan, J. F.; DeGroot, M. W. Large Semiconductor Molecules. In *The Chemistry of Nanomaterials: Synthesis, Properties and Applications*, 1st ed.; Rao, C. N. R., Mueller, A., Cheetham, A. K., Eds.; Wiley-VCH: Weinheim, Germany, 2004; Vol. 2, pp 418−451.
(62) Porezag, D.; Frauenheim, Th.; Köhler, Th.; Seifert, G.; Kaschner, R. *Phys. Rev. B* **1995**, *51*, 12947–12957.
(63) Elstner, M.; Porezag, D.; Jungnickel, G.; Elsner, J.; Haugk, M.; Fraunheim, Th.; Suhai, S.; Seifert, G. *Phys. Rev. B* **1998**, *58*, 7260–7268.
(64) Niehaus, Th.; Suhai, S.; DellaSala, F.; Lugli, P.; Elstner, M.; Seifert, G.; Frauenheim, Th. *Phys. Rev. B* **2001**, *63*, 085108.
(65) Seifert, G. *J. Phys. Chem. A* **2007**, *111*, 5609–5613.
(66) Aradi, B.; Hourahine, B.; Fraunheim, Th. *J. Phys. Chem. A* **2007**, *111*, 5678–5684.
(67) Bhattacharya, S. K.; Deodhar, P. A.; Viswanatha, R.; Kshirsagar, A. *J. Phys.: Condens. Matter* **2010**, *22*, 295304.
(68) Hohenberg, P.; Kohn, W. *Phys. Rev.* **1964**, *136*, B864.
(69) Kohn, W.; Sham, L. J. *Phys. Rev.* **1965**, *140*, A1133.
(70) Perdew, J. P.; Burke, K; Ernzerhof, M. *Phys. Rev. Lett.* **1996**, *77*, 3865–3868.
(71) Monkhorst, H. J.; Pack, J. D. *Phys. Rev. B* **1976**, *13*, 5188–5192.
(72) Soler, J, M; Artacho, E.; Gale, J. D.; Garcia, A.; Junquera, J.; Ordejon, P.; Sanchez-Portal, D. *J. Phys.: Condens. Matter* **2002**, *14*, 2745–2779.
(73) Troullier, N.; Martins, J. L. *Phys. Rev. B* **1991**, *43*, 1993–2006.
(74) Lee, C.; Yang, W.; Parr, R. G. *Phys. Rev. B* **1993**, *37*, 785–789.
(75) Becke, A. D. *J. Chem. Phys.* **1998**, *88*, 1053–1062.
(76) Frisch, M. J.; Trucks, G. W.; Schlegel, H. B.; G. E.Scuseria, Robb, M. A.; Cheeseman, J. R.; Montgomery, J. A., Jr.; Vreven, T.; Kudin, K. N.; Burant, J. C.; Millam, J. M.; Iyengar, S. S.; Tomasi, J.; Barone, V.; Mennucci, B.; Cossi, M.; Scalmani, G.; Rega, N.; Petersson, G. A.; Nakatsuji, H.; Hada, M.; Ehara, M.; Toyota, K.; Fukuda, R.; Hasegawa, J.; Ishida, M.; Nakajima, T.; Honda, Y.; Kitao, O.; Nakai, H.; Klene, M.; Li, X.; Knox, J. E.; Hratchian, H. P.; Cross, J. B.; Adamo, C.; Jaramillo, J.; Gomperts, R.; Stratmann, R. E.; Yazyev, O.; Austin, A. J.; Cammi, R.; Pomelli, C.; Ochterski, J. W.; Ayala, P. Y.; Morokuma, K.; Voth, G. A.; Salvador, P.; Dannenberg, J. J.; Zakrzewski, V. G.; Dapprich, S.; Daniels, A. D.; Strain, M. C.; Farkas, O.; Malick, D. K.; Rabuck, A. D.; Raghavachari, K.; Foresman, J. B.; Ortiz, J. V.; Cui, Q.; Baboul, A. G.; Clifford, S.; Cioslowski, J.; Stefanov, B. B.; Liu, G.; Liashenko, A.; Piskorz, P.; Komaromi, I.; Martin, R. L.; Fox, D. J.; Keith, T.; Al-Laham, M. A.; Peng, C. Y.; Nanayakkara, A.; Challacombe, M.; Gill, P. M. W.; Johnson, B.; Chen, W.; Wong, M. W.; Gonzalez, C.; Pople, J. A. *Gaussian 03*, Revision E.01; Gaussian, Inc.: Wallingford, CT, 2004.
(77) Stark, R. W.; Falicov, L. M. *Phys. Rev. Lett.* **1967**, *19*, 795.
(78) Daniuk, S.; Jarlborg, T.; Kontrym-Sznajd, G.; Majsnerowski, J.; Stachowiak, H. *J. Phys.: Condens. Matter* **1989**, *1*, 8397–8406.
(79) Kittel, C. Crystal Binding. In *Introduction to Solid State Physics*, 7th ed.; Wiley: New York, 1995; pp 57.
(80) McCann, D. R.; Cartz, L. *J. Appl. Phys.* **1972**, *43*, 4473.
(81) Lingelbach, W.; Stuke, J; Weiser, G.; Treusch, J. *Phys. Rev. B* **1972**, *5*, 243.
(82) Ghosh, P.; Upadhyay, K.; Waghmare, U. V. *Phys. Rev. B* **2007**, *75*, 245437.
(83) Biering, S.; Hermann, A.; Furthmuller, J.; Schwerdtfeger, P. *J. Phys. A* **2009**, *113*, 12427–12432.
(84) Dou, Y.; Egdell, R. G.; Law, D. S. L.; Harrison, N. W.; Searle, B. G. *J. Phys.: Condens. Matter* **1998**, *10*, 8447–8458.
(85) Reshak, A. H. *J. Chem. Phys.* **2006**, *124*, 104707–6.
(86) Huang, M.-Z.; Ching, W. Y. *Phys. Rev. B* **1993**, *47*, 9449.
(87) Huang, M.-Z.; Ching, W. Y. *Phys. Rev. B* **1993**, *47*, 9464.
(88) Wei, S.-H.; Zhang, S. B. *Phys. Rev. B* **2000**, *62*, 6944.
(89) Hannachi, L.; Bouarissa, N. *Physica B* **2009**, *404*, 3650–3654.
(90) Christensen, N. E.; Christensen, O. B. *Phys. Rev. B* **1986**, *33*, 47466–47474.
(91) Zakharov, O.; Rubio, A.; Blase, X.; Cohen, M. L.; Louie, S. G. *Phys. Rev. B* **1994**, *50*, 10780–10787.
(92) Hosseini, S. M. *Physica B* **2008**, *403*, 1907–1915.
(93) Duke, C. B.; Wang, Y. R. *J. Vac. Sci, Technol. B* **1988**, *6*, 1440–1443.
(94) Wang, Y. R.; Duke, C. B. *Surf. Sci.* **1987**, *192*, 309.
(95) Wang, Y. R.; Duke, C. B. *Phys. Rev. B* **1987**, *36*, 2763.
(96) Wang, Y. R.; Duke, C. B. *Phys. Rev. B* **1988**, *37*, 6417.
(97) Siemens, B.; Domke, C.; Ebert, Ph.; Urban, K. *Phys. Rev. B* **1997**, *56*, 12321–12326.
(98) Li, S.; Yang, G. W. *J. Phys. Chem. C* **2010**, *114*, 15054–15060.
(99) Huang, S.-P.; Cheng, W.-D.; Wu, D.-S.; Hu, J.-M.; Shen, J.; Xie, Z.; Zhang, H.; Gong, Y.-J. *Appl. Phys. Lett.* **2007**, *90*, 031904.
(100) Xiong, Y.; Xie, Y.; Yang, J.; Zhang, Z.; Wu, C.; Du, G. *J. Mater. Chem.* **2002**, *12*, 3712.
(101) Kwon, S. J.; Choi, Y. J.; Park, J. H.; Hwang, I. S.; Park, J. G. *Phys. Rev. B* **2005**, *72*, 205312.
(102) Köhler, C.; Seifert, G.; Gerstmann, U.; Elstner, M.; Overhof, H.; Frauenheim, T. *Phys. Chem. Chem. Phys.* **2001**, *3*, 5109.
(103) Simöes, J. A. M.; Beauchamp, J. L. *Chem. Rev.* **1990**, *90*, 629–688.
(104) Dutton, W. A.; Cooper, W. C. *Chem. Rev.* **1966**, *66*, 657–675.

(105) Madelung, O. M. Tetrahedrally bonded elements and compounds. In *Semiconductors: Data Hand Book*, 3rd ed.; Springer: Berlin, 2004; pp 218.
(106) Wired Chemist. http://www.wiredchemist.com/chemistry/data (accessed Dec 8, 2010).
(107) Greene, T. M.; Brown, W.; Andrews, L.; Downs, A. J.; Chertihin, G. V.; Runeberg, N.; Pyykko, P. *J. Phys. Chem.* **1995**, *99*, 7925–7934.
(108) Greenwood, N. N.; Earnshaw, A. Selenium, Tellurium and Polonium. In *Chemistry of the Elements*, 2nd ed.; Pergamon Press: Oxford, U.K., 1997; p 766.
(109) Balasubramanian, K.; Liao, M. Z. *J. Phys. Chem.* **1988**, *92*, 4595–4599.
(110) Gabuda, S. P.; Kozlova, S. G. *J. Phys. Chem. B* **2006**, *110*, 18091–18092.
(111) Gibson, S. T.; Greene, J. P.; Berkowitz, J. *J. Chem. Phys.* **1986**, *85*, 4815–4824.
(112) Carson, A. S.; Hartley, K.; Skinner H. A. The Bond Dissociation Energies of Cd-CH_3 in $Cd(CH_3)_2$, and of CH_3-I in CH_3 I. *Proc. R. Soc. London, Ser. A* **1949**, *195*, 500−512. http://www.jstor.org/stable/98237 (accessed 02/07/2010).
(113) Scott, J. D.; Causley, G. C.; Russell, B. R. *J. Chem. Phys.* **1973**, *59*, 6577.
(114) Goldish, E.; Hergberg, K.; Marsh, R. E.; Schomaker, V. *J. Am. Chem. Soc.* **1955**, *779*, 2948–2949.